Universitat Politècnica de Catalunya (UPC)
Universitat Autònoma de Barcelona (UAB)
Universitat de Barcelona (UB)
Institut de Ciències Fotòniques (ICFO)

http://www.photonicsbcn.eu

Master in Photonics

MASTER THESIS WORK

A PLASMONIC ACCURACY BIOSENSOR USING A SINGLE LASER DIODE

Paula Bañares Palacios

Supervised by Dr. Santiago Royo Royo, (CD6)

Presented on date 7th September 2016

Registered at

Escola Tècnica Superior d'Enginyeria de Telecomunicació de Barcelona

A plasmonic accuracy biosensor using a single laser diode

Paula Bañares Palacios

Centre for Sensors, Instruments and Systems Development (CD6), Politechnic University of Catalonia (UPC Barcelona Tech), Terrassa E08222, Spain

E-mail: paula.banares@estudiant.upc.edu

July 2016

Abstract. A theoretical model was implemented to obtain the total specular reflection of a variable external multicavity for out of normal incidence and different polarisations. The model was theoretically and experimentally validated and a further analysis was applied to the study of the stability of the SMI signal. It was found that out of normal incidence, or the use of different polarisations does not affect the quality of the signal in a relevant manner.

Keywords: Self Mixing Interferometry, Polarisation, Multicavity analysis, Brewster's incidence, Biosensor

1. Introduction

Currently, a very successful approach for high accuracy refractive index sensors are those based on surface plasmon resonance (SPR). An alternative was presented in a previous research work [1] which uses a lower cost, more compact set-up based on self-mixing interferometry (SMI), which was shown measures changes of refractive index of 10^{-5}.

The self-mixing interferometry technique is based on the effect produced on the electromagnetic field inside the laser cavity when part of the output of the laser is re-injected after reflection. Changes in the optical path of the beam outside the laser cavity will produce changes in the intracavity field that can be measured and later processed for the extraction of information, such as the displacement of the target or other changes in the optical path, in particular changes in the refractive index of the external medium. Such changes in the intracavity field are obtainable through the SMI signal, which can be measured via a photodiode that is placed next to the laser cavity. It recolects laser light coming back towards the cavity and is able to measure small changes in the output power if properly amplified.

Many factors affect the SMI signal that is obtained, such as the reflectivity of the target, its distance to the laser, the ambient temperature or any small vibrations that the set-up could undergo. In general, any potential change to the optical path of

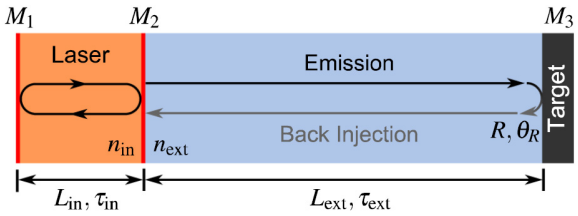

Figure 1: Three mirror model for self mixing interferomatry. The laser cavity is represented in orange with refractive index n_{in}, length L_{in} and roundtrip propagation time τ_{in}. The external cavity is represented in blue with refractive index n_{ext}, length L_{ext} and roundtrip propagation time τ_{ext}. Mirrors M_1 and M_2 control laser gain in the laser cavity, and mirror M_3 represents the surface of the target, with reflectivity R. The light comes back into the laser cavity through mirror M_2 interacting with the laser field inside the cavity [3].

the light between target and laser affects the stability of the signal. Experimentally, it is demanding to keep these parameters constant to get information of only one of them, leading to the constant search of configurations which could improve the systems. Since the precision of the refractive index measurements reported [1] must be really high, special care must be taken to obtain a stable SMI signal at this levels. Polarised incidence at Brewster's angle onto an external multicavity system was proposed in order to eliminate internal reflections and make the cavity "transparent" to the light in one direction of polarization. In this work we will explore both out of normal incidence and polarisation effects in order to know if they can be used to improve the SMI signal stability, which can later be applicable to refractive index measurements.

2. Theoretical model

In 1980, Lang and Kobayashi (LK)[2] developed mathematical equations for the electric field and the carrier density that describe the laser dynamics under optical feedback. An optical feedback scheme is shown in Fig. 1 [3]. Either operating using LK equations or from the equivalent cavity model shown in Fig. 1, the excess phase equation [3] presented in eqn. 1 can be obtained. In it, ϕ_s accounts for the phase accumulated in the external cavity as if there was no optical feedback (phase stimulus), ϕ_{FB} accounts for the actual phase accumulated in the external cavity (phase response), α is the linewidth enhancement factor and C is the feedback level, dependent upon the coupling strength between the laser and the external cavity, the internal and external time of flight and the linewidth enhancement factor α. The optical output power can be then obtained from ϕ_{FB}, since it depends on it through a sinusoidal function. The shape of this sinusoidal function is deformed depending on the feedback level [4]. A feedback of $C \simeq 1$ is preferred for refractive index change measurements in order to improve SNR, prevent fringe loss, limit hysteresis effects and detect the direction of displacement.

$$\phi_{FB} - \phi_s + C \sin\left(\phi_{FB} + \arctan\alpha\right) = 0 \tag{1}$$

In order to work with this model it is necessary to know the reflectivity of the target. Since we want to measure changes of refractive index in a liquid, we need to maintain

Interface	$R_p(\%)$	θ_+ (°)	θ_-(°)	range (°)
Air-Glass	1	64.3	44.3	20
Glass-Water	0.4	49.2	10.4	48.8
Air-Aluminium	1	84.1	81.2	2.9
Water-Aluminium	1	82.2	78.3	3.9

Table 1: Brewster's angle sensitivity. θ_+ and θ_- give the angle after and before Brewster's angle respectively at which the reflectivity goes up to a value given by R_p. The range is the subtraction of θ_+ and θ_-, showing the precision which would be needed for Brewster's angle incidence.

the substance in a recipient where at least the front surface is glass, with the laser pointing at it. All the possible practical configurations for refractive index mesurements involve a multiple external cavity, which complicates the simple approach presented in Fig.1. Thus, our first approach was to implement a program in Matlab to calculate the total reflectivity of a variable external cavity that can be chosen as input. Such model was based on the Pochi Yeh's model for multilayer optics [5]. It is a matrix model that accounts for multiple reflections inside the different parallel cavities, returning the total specular reflection of a compound structure for both S and P polarisations at any specific angle of incidence.

2.1. Normal incidence and Brewster's angle incidence

As a first step, reflectivity curves dependent on the incidence angle between two different media were studied, to see how fast would the reflectivity increase when going apart from Brewster's angle, and whether this sensitivity could prevent us from using Brewster's angle incidence in practice. Incidence at Brewster's angle is expected to eliminate to some degree the unwanted reflections inside the multiple cavities, given we only take into account the polarisation parallel to the plane of incidence (P polarisation). Supposing we would like to measure the refractive index of water, an Air-Glass-Water-Glass-Air-aLuminium ($AGWGAL$) structure or an Air-Glass-Water-aLuminium ($AGWL$) structure would be used in practice, with water between two glass layers or between a glass and an aluminium layer. The involved interfaces and their inverses were chosen for the calculation of the reflectivity curves (with *inverse* meaning the back to front propagation of the light). The curves show that the ones involving glass or water presented flatter curves around Brewster's angle than the ones involving the aluminium surface (Table 1), so a larger incidence range is available. The inverse interfaces present curves similar to the correspondent direct interfaces, so their results are not shown.

Afterwards, using Pochi Yeh's model the reflectivies for the complete given structures (AGWGAL and AGWL) were simulated for incidence at Brewster's angle for the air-glass interface (55.6°, 56° in the simulations). The rest of the parameters used were: air layer thickness $d_a = 100e-3$ m, glass thickness $d_g = 1e-3$ m and water layer thickness $d_w = 0.5e-3$ m. The results are given in Table 2. Since AL and WL

Structure	$\theta(^o)$	θ on Al	$R_s(\%)$	$R_p(\%)$
AGWGAL	0	normal	60.95	60.95
	56	inclined	88.85	38.32
AGWL	0	normal	38.24	38.24
	56	inclined	33.32	42.57

Table 2: Specular reflectivities for structures with aluminium.

Structure	$\theta(^o)$	$R_s(\%)$	$R_p(\%)$
AGWGAP	0	10.98	10.98
	56	49.80	0.14
AGWP	0	1.57	1.57
	56	6.82	0.26

(a)

Structure	$\theta(^o)$	$R_s(\%)$	$R_p(\%)$
AGWGAT	0	9.80	9.80
	56	47.89	0.14
AGWT	0	3.12	3.12
	56	8.24	0.59

(b)

Table 3: Specular reflectivities for structures with PVC (P) as reflective surface (a) and teflon (T) as reflective surface (b).

interfaces present a Brewster's angle much different from that of AG and GW, and also a larger sensitivity, we see how incidence at 56° for P polarisation does not significantly lower the reflectivity of the structure.

To cope with this effect, we propose a reflecting surface with refractive index closer to that of water and glass, and we find that PVC (P) has a refractive index of n=1.52-1.54 [6], and teflon (T) of n=1.35-1.38 [7]. The same simulations are run with these reflective surfaces, with the results shown in Table 3. In this case we can see how, for P polarisation, reflectivities go down to close to 0%, so a significant effect in the elimination of back reflections in one of the components of polarization is obtained.

2.2. Effect of variable incidence angle θ_{inc}, distance of cavity d and refractive index n

Modifying the program used for the previous simulations, three other simulations for reflectivities of the structures presented above involving varying incidence angle, distance of the air cavity and refractive index of the water cavity were performed. An example of the results can be seen in Fig. 2 for varying θ_{inc} and Fig. 3 for varying distance and refractive index.

In Fig. 2 it can be seen that the reflectivity varies in a wide range of values inside a small range of incidence for the S polarisation, while P polarisation curves present a much flatter profile. The shape of the curves is produced by interferences of the light within the multiple cavities. Regarding the effects of varying distance and refractive index, in Fig. 3 it can also be seen that the range of reflectivities for the S polarisation is really wide with changes between roughly $5 - 55\%$ in both cases. Since we have

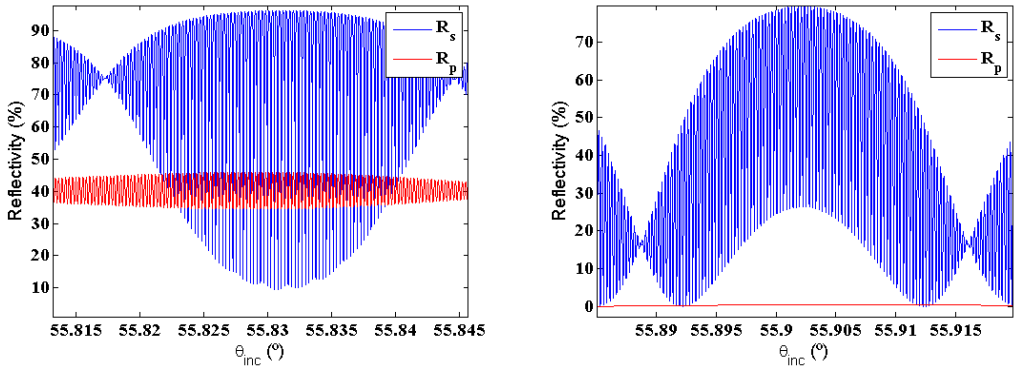

(a) (b)

Figure 2: Reflectivities for varying θ_{inc}. (a) corresponds to an AGWGAL structure, (b) to an AGWGAP structure. Incidence is shown around Brewster's angle for air-glass, 55.6º, in both figures.

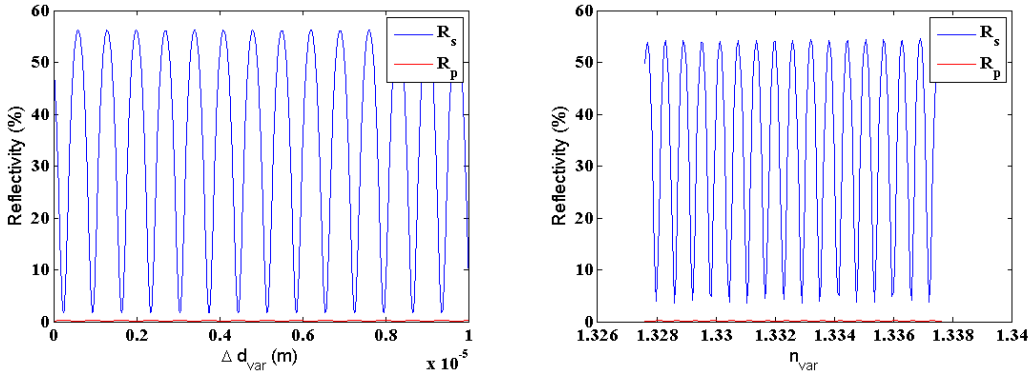

(a) (b)

Figure 3: Reflectivities for varying distance of the air cavity d_A (a) and varying refractive index n_W (b).

Brewster's angle incidence, P polarisation remains close to zero. All this shows that using P polarisation will potentially lead to more stable SMI signals.

3. Validation of the theoretical model

3.1. Theoretical validation

In order to validate the model we perform a double check, both from a theoretical and experimental approaches. Theoretically, we compare the transmission curves obtained from the well-known Airy's formulas [8], which can only be used for three different media, and the Pochi Yeh's model [5] we just implemented in the code, which can be used for a variety of different structures. Both models take into account multiple reflections in internal cavities. We use a simple Air-Glass-Air (AGA) structure and varying θ_{inc} between -70^{o} and 70^{o}, obtaining symmetrical curves. An example of each model is

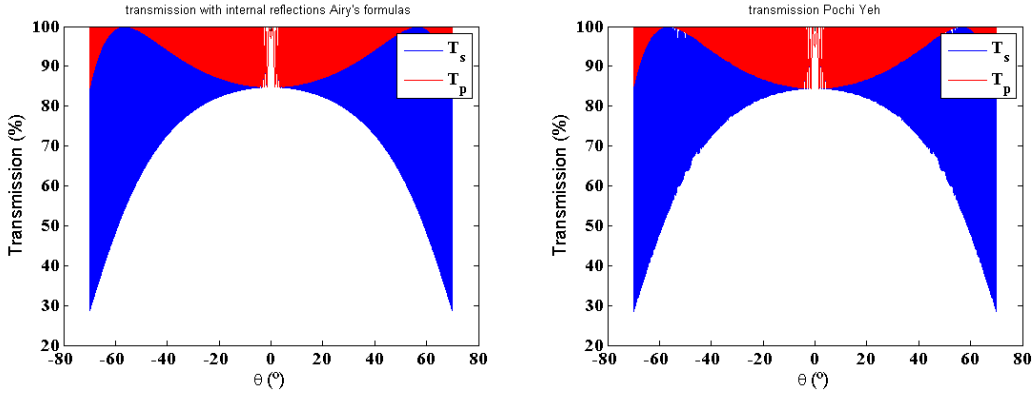

(a) (b)

Figure 4: Theoretical model validation. Transmission with Pochi Yeh's matrix method (*a*) and with Airy's formulas (*b*) for an AGA structure.

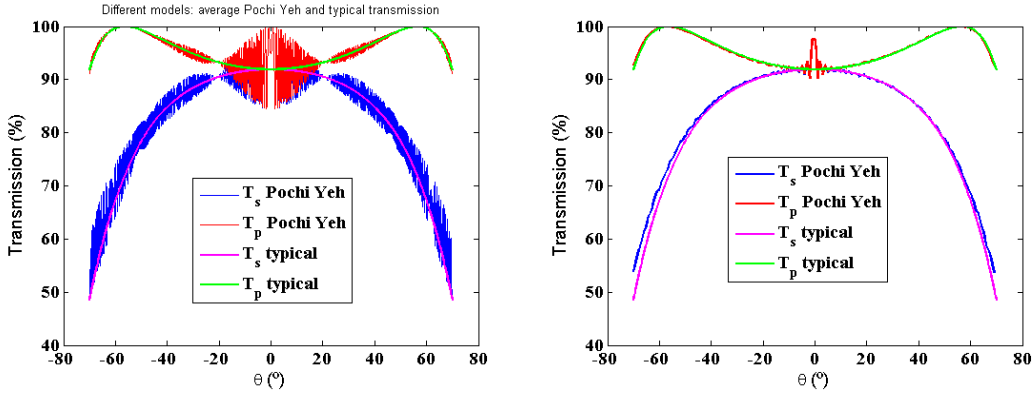

(a) (b)

Figure 5: Model validation. Typical transmission curves and average for 0.1º (*a*) and for 1º (*b*) of Pochi Yeh's matrix method transmission.

shown in Fig. 4, where it can be seen that both curves are equivalent.

Typical transmission curves ("typical" meaning the ones obtained when measuring transmission through a glass) present a different profile from the ones observed in Fig. 4. An average value of Pochi Yeh's curves taking as ranges 1º, 0.5º, 0.25º and 0.1º was performed to account for imperfect collimation effects and compared to typical transmission curves. The results can be seen in Fig. 5 for 0.1º and 1º. Typical transmission curves are calculated by obtaining the Fresnel coefficients of each interface from the refractive index values and multiplying the final transmissions of each interface (so they do not take into account multiple internal reflections). In the figure it can be seen that the larger the chosen averaging range, the better the fit to the typical transmission curves, since a higher number of complete oscillations is accounted for the statistics. Around normal incidence the oscillations are more appreciated, since they are wider than at angles far from it.

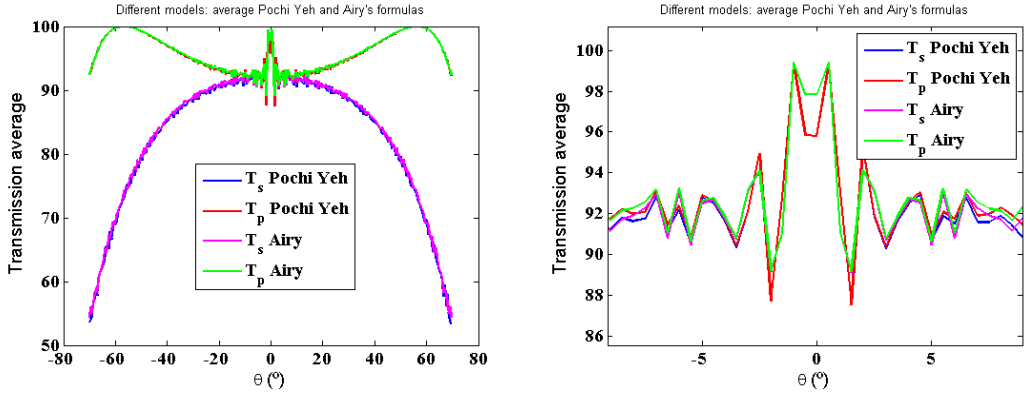

Figure 6: Model validation. Averaged Airy's formulas transmission and Pochi Yeh's matrix method transmission for 0.5º. (*b*) shows a close-up of (*a*) around normal incidence.

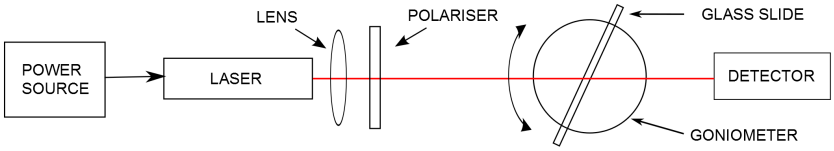

Figure 7: Experimental set-up used for transmission curves measurement.

Both Pochi Yeh's and Airy's formulas average for 0.5º are also compared in Figure 6, where both incidence between -70º and 70º and a close up around normal incidence can be observed. In both schemes the fit is pretty good, with minor deviations.

3.2. Experimental model validation

Once the theoretical validation of the multicavity model was established, we performed an experimental validation. A set-up was built in order to be able to measure transmission through glass, in what would be an Air-Glass-Air (AGA) cavity. A Fabry-Perot (*FP*) laser (HL7851G) was used for the measurements. A scheme of the set-up is shown in Fig. 7. The measurements were done focusing the beam at the detector with a (A110TM-B) lens and collimating the beam with a (LTN330-B) lens, both placed right at the output of the laser. The desired polarisation was forced placing a linear polariser between the lens and the glass surface. In Fig. 8 the results are shown. It can be seen how the curves taken with a focused beam present a better fit for higher ranges of the averaged Pochi Yeh's curve (0.5º). In the case of the collimated beam, the oscillations obtained with the models that take into account internal reflections can also be observed in the experimental curves, and it is found that the best fit is found to an averaged range of angles of 0.2º. This happens because with the focused beam incidence happens at a range of angles of roughly ±0.6º, therefore it requires a larger averaged range than the collimated beam measurements. Both experimental and theoretical models present comparable features, showing the validity of the model.

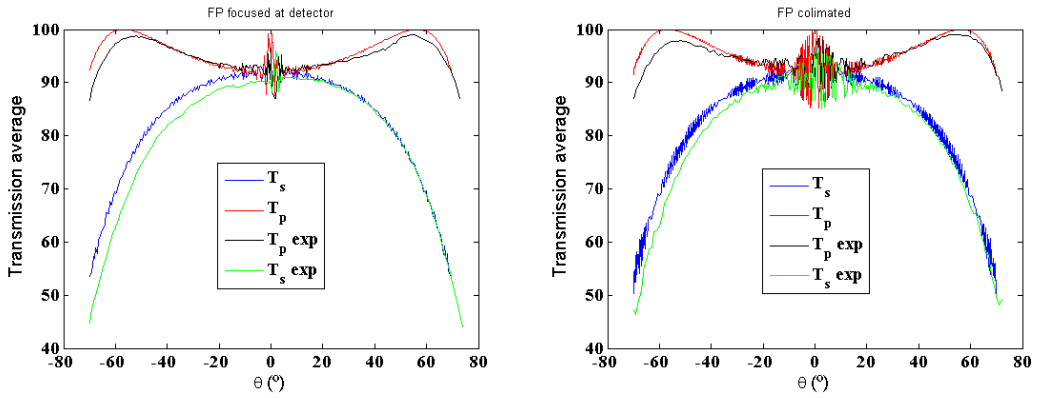

Figure 8: Experimental transmission curves compared to Pochi Yeh's matrix method. (*a*) shows the curves taken with a FP focused at the detector and averaged Pochi Yeh's for 0.5º. (*b*) shows the transmission curves of the same laser with a collimated beam and averaged Pochi Yeh's for 0.2º.

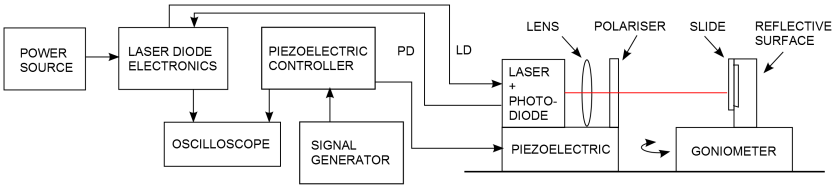

Figure 9: Experimental set-up used for measurement of SMI signal stability.

4. Stability of the experimental SMI signal

Once we have a model that calculates the specular reflectivity of the multiple cavities that appear for refractive index measurements, we try to obtain information on stability which will help to obtain those measurements with better accuracy. Since the reflectivity of the target severely influences the SMI signal, the transmission curves are analysed. From the ones presented in Fig. 8, we expect the stability of the signal for a focused beam around normal incidence to be higher than for a collimated beam. We also expect higher stability at high angles of incidence for both the focused and collimated beams.

Measurements of the SMI signal were taken using the FP laser. A PVC piece was applied as reflective surface, where a sandpaper was used to roughen it to obtain feedback at high angles of incidence. A scheme of the set-up is shown in Fig. 9. Measurements were taken for a focused and a collimated beam and for both polarisations, around 0º, 5º, 10º, 20º, 40º and 56º. They were taken in a range of ±2º, every 0.5º, for the given angles, giving 9 measurements in total for each set of angles.

The SMI signals were analysed in three ways: in the first one, the amplitude of the signal was measured, as it was expected to be a factor that would give information about the signal quality, but it was found to be uncorrelated. In the second, the expected number of fringes was compared to the actual one (telling us if the SMI signal was clear enough to overcome noise). In the third one, since we know that the fringes should all be

		0º		5º		40º		56º	
		$\#frin.$	$\downarrow frin.$	$\#frin.$	$\downarrow frin.$	$\#frin.$	$\downarrow frin.$	$\#frin.$	$\downarrow frin.$
P_{pol}	Exp.	95	0	95	0	95	0	95	0
	Avg.	97 ± 0	6 ± 6	97 ± 1	8 ± 12	95 ± 3	17 ± 12	97 ± 1	8 ± 7
	% Err.	2.3	6.1	2.3	8.8	0.5	17.8	1.99	8.4
S_{pol}	Exp.	95	0	95	0	95	0	95	0
	Avg.	97 ± 1	9 ± 9	96 ± 1	8 ± 7	97 ± 1	5 ± 5	97 ± 1	5 ± 6
	% Err.	3.2	9.2	2.1	8.5	3.2	5.7	3.2	5.4

Table 4: Stability signal for a focused beam at various incidence angles. $\#frin.$ refers to the total number of fringes in the signal. $\downarrow frin.$ refers to the number of fringes pointing towards the wrong direction. *Exp.* refers to the expected number of fringes, and *Avg.* to the average obtained for the nine measurements in each set.

		0º		5º		40º		56º	
		$\#frin.$	$\downarrow frin.$	$\#frin.$	$\downarrow frin.$	$\#frin.$	$\downarrow frin.$	$\#frin.$	$\downarrow frin.$
P_{pol}	Exp.	86	0	86	0	86	0	86	0
	Avg.	96 ± 15	51 ± 16	105 ± 17	53 ± 10	116 ± 8	59 ± 10	113 ± 13	58 ± 14
	% Err.	12.1	60	22	62	34	68	32	67
S_{pol}	Exp.	86	0	86	0	86	0	86	0
	Avg.	98 ± 8	52 ± 12	97 ± 29	44 ± 14	110 ± 15	53 ± 10	114 ± 13	59 ± 8
	% Err.	14.3	60	12.9	52	28	61	32	69

Table 5: Stability signal for a collimated beam at various incidence angles. $\#frin.$ refers to the total number of fringes in the signal. $\downarrow frin.$ refers to the number of fringes pointing towards the wrong direction. *Exp.* refers to the expected number of fringes, and *Avg.* to the average obtained for the nine measurements in each set.

bended in the same direction because of the type of movement the piezoelectric applies, the number of fringes pointing in direction opposite to that expected after processing was counted and compared to the expected one. The less fringes in the wrong direction we find, the higher the quality of the obtained signal. Processing of the signal was made with the same parameters for each the set of data, since we are studying its stability. Results for the extreme angles and both polarisations are shown in Table 4 for the focused beam and in Table 5 for the collimated beam. Standard deviation is used to estimate the average uncertainty, and the percentage of error is calculated from the average obtained value and that expected, for a clearer understanding of the data.

The first thing to notice is that, for the focused beam, the errors in the total number of fringes (#) are small for the different angles of incidence. This means that in all the cases we obtain a signal with clear fringes, but also that no discrimination is possible between different angles. With regards to the inclination of the fringes ($\downarrow$), it can be seen that the errors are similar for the different angles and polarisations, without any noticeable improvement for larger angles. From both analysis we can conclude that there would be no significant difference between measuring the signal at different angles or at different polarisation planes for a focused beam, obtaining good results in all cases.

In the case of the collimated beam we find significantly different results. With regards to the total number of fringes (#), we find that the errors increase with the angle of incidence. When we obtain a different number of fringes than expected, it means that the signal presents too much noise and the processing algorithm is unable to find well defined fringes. Regarding the inclination of the fringes (↓), we see really high errors in all cases. This happens because the detected "fringes" point randomly in both directions. From all this we see that a collimated beam is not useful to obtain the SMI signal even at high angles, where we expected the feedback to be more stable.

5. Conclusion

A theoretical model for a variable external multicavity system based on Pochi-Yeh theory was implemented and validated. A preliminar analysis suggested that out of normal incidence could provide a more stable SMI signal, specially for polarisation parallel to the plane of incidence (P), which showed flatter curves, and in the case of a collimated beam, where reflectivity showed great variability around normal incidence. In particular, incidence at Brewster's angle promised to reduce undesired backrreflection in one polarization plane.

A detailed model based in Pochi Yeh theory was implemented to simulate multiple external cavities in the SMI sensor, and showed its validity to take into account multiple reflections inside the cavity. The model was coded and validated both from the comparison with a simple multicavity system based in Airy equations, and later validated from experimental measurements. Despite the success in the preparation of the model, experimentally it was not found that either polarisation or incidence at different angles improved the quality of the signal. The main experimental conclusion drawn is the confirmation of the unstability of signals from collimated beams at any angle of incidence when compared with focused beams, which show much better quality.

References

[1] Vidakis A 2015 *Developing a laser-based biosensor with plasmonic accuracy* Master's thesis Technical University of Catalonia UPC-BarcelonaTech

[2] Lang R and Kobayashi K 1980 *IEEE Journal of Quantum Electronics* **16** 347–355 ISSN 0018-9197

[3] Taimre T, Nikolić M, Bertling K, Lim Y L, Bosch T and Rakić A D 2015 *Adv. Opt. Photon.* **7** 570–631

[4] Donati S, Giuliani G and Norgia M 2004 Self-mixing techniques for sensing applications *Proc. 4th Optoelectronic Distance/Displacement Measurements and Applications Conf* pp 213–234

[5] Yeh P 2005 *Optical waves in layered media* (Wiley)

[6] `https://www.akelastomer.com/eng/guide/g_asaflex_kussetsu.html` Web 07-06-2016

[7] French R H, Rodríguez-Parada J M, Yang M K, Derryberry R A, Lemon M F, Brown M J, Haeger C R, Samuels S L, Romano E C and Richardson R E 2009 Optical properties of materials for concentrator photovoltaic systems *Photovoltaic Specialists Conference (PVSC), 2009 34th IEEE* pp 000394–000399 ISSN 0160-8371

[8] BEASaleh M 2014 *Fundamentals of photonics* (Wiley)